The Meteoritical Society

Meteoritics & Planetary Science 53, Nr 6, 1238–1251 (2018)
doi: 10.1111/maps.13069

Origin and significance of cosmogenic signatures in vesicles of lunar basalt 15016

David V. BEKAERT[1*], Guillaume AVICE[1,2], and Bernard MARTY[1]

[1]Centre de Recherches Pétrographiques et Géochimiques, UMR 7358 CNRS—Université de Lorraine, 15 rue Notre Dame des Pauvres, BP 20, 54501 Vandoeuvre-lès-Nancy, France
[2]Present address: Division of Geology and Planetary Sciences, California Institute of Technology, 1200 E. California Blvd, Pasadena, California 91125, USA
[*]Corresponding author. E-mail: dbekaert@crpg.cnrs-nancy.fr

(Received 22 December 2016; revision accepted 05 February 2018)

Abstract–Lunar basalt 15016 (~3.3 Ga) is among the most vesicular (50% by volume) basalts recovered by the Apollo missions. We investigated the possible occurrence of indigenous lunar nitrogen and noble gases trapped in vesicles within basalt 15016, by crushing several cm-sized chips. Matrix/mineral gases were also extracted from crush residues by fusion with a CO_2 laser. No magmatic/primordial component could be identified; all isotope compositions, including those of vesicles, pointed to a cosmogenic origin. We found that vesicles contained ~0.2%, ~0.02%, ~0.002%, and ~0.02% of the total amount of cosmogenic ^{21}Ne, ^{38}Ar, ^{83}Kr, and ^{126}Xe, respectively, produced over the basalt's 300 Myr of exposure. Diffusion/recoil of cosmogenic isotopes from the basaltic matrix/minerals to intergrain joints and vesicles is discussed. The enhanced proportion of cosmogenic Xe isotopes relative to Kr detected in vesicles could be the result of kinetic fractionation, through which preferential retention of Xe isotopes over Kr within vesicles might have occurred during diffusion from the vesicle volume to the outer space through microleaks. This study suggests that cosmogenic loss, known to be significant for ^{3}He and ^{21}Ne, and to a lesser extent for ^{36}Ar (Signer et al. 1977), also occurs to a negligible extent for the heaviest noble gases Kr and Xe.

INTRODUCTION

Noble gases in lunar samples are dominated by solar wind and cosmic ray produced contributions, with minor additions of isotopes produced by natural radioactivity (e.g., ^{40}Ar produced by the decay of ^{40}K, or $^{131–136}$Xe isotopes produced by the fission of ^{244}Pu and ^{238}U). While solar contributions in lunar rocks may be used as an archive of the history of solar composition and activity (Wieler 2016), cosmogenic isotopes are extensively used for samples exposure dating (Eugster [2003] and references therein). This method relies on the determination of the amounts of cosmogenic isotopes that were produced in minerals during exposure of the parent rock to space cosmic rays, mainly high-energy H^+ particles.

Although the possible detection of a cometary signature in lunar anorthosite samples has been recently reported (Bekaert et al. 2017), the search for an indigenous lunar (i.e., nonsolar, radiogenic, fissiogenic, or cosmogenic) noble gas component has resisted decades of investigation. Nevertheless, the presence of highly vesicular basalts on the Moon testifies to the fact that episodes of gas-rich lunar magma eruption have occurred. Mare basalts, derived from the lunar mantle, thus represent key samples with which to investigate the inventory of volatile elements in the lunar interior. Here, we test the possibility that indigenous noble gases have remained trapped in vesicles of the highly vesicular basalt 15016 since its eruption. Although several possible sources of gases have been suggested for the origin of lunar basalt vesiculation (e.g., radiogenic ^{40}Ar, N_2, fluorine compounds, sulfur, solar wind gases, and/or—more reliably—carbon monoxide [Goldberg et al. 1976]), the gases associated with the basalt 15016 parent magma probably had a composition close to 46% O, 42% C,

a)

Crushing experiments			
Sample	LS	LR	LP
Mass (mg)	414.1	673.4	818.9
Analyses	He, Ne, Ar, N	Ar, Kr, Xe	
Mass spec.	VG5400	Helix MC	
# crush. steps	10	2	

CO_2 laser extraction				
Sample	LP crushing residues			
Mass (mg)	2.629	5.909	2.673	4.513
Analyses	He, Ne, Ar, N		Kr, Xe	
Mass spec.	VG5400		Helix MC	
# heating steps	3	2	1	1

b)

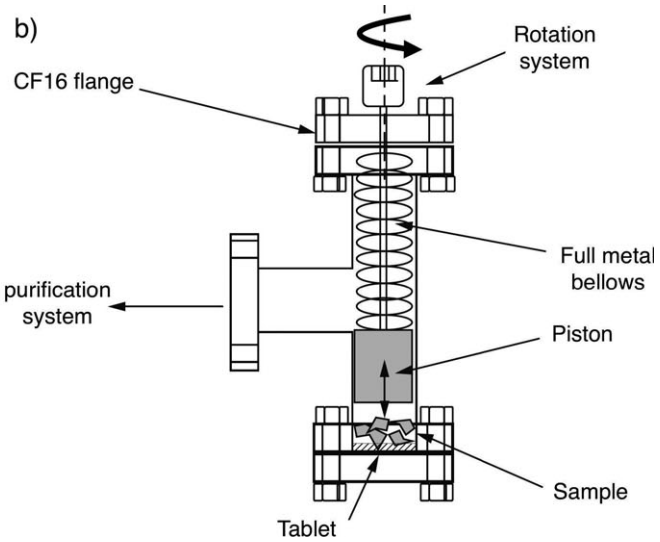

Fig. 1. a) Samples and analytical techniques used in this study. # crush. steps: number of crushing steps carried out on the corresponding sample(s), # heating. steps: number of heating steps performed for each crushing residue. b) Schematic drawing of the manually driven crushing system used in this study, adapted from Zimmermann and Marty (2014).

and 12% H (Barker 1974), the most plausible cause of vesiculation being related to CO release/exsolution (Sato 1979; Garvin et al. 1982; Colson 1993; Meyer 2009). basalt 15016 was formed by very quick cooling, at low pressure, of a basaltic magma originating from a depth of >250 km in the Moon (Meyer 2009).

In this study, we crushed basalt 15016 under vacuum and analyzed the elemental and isotopic compositions of noble gases and nitrogen contained in the vesicles but find no evidence for a contribution from a magmatic/indigenous component. Because of its large exposure duration (~300 Ma; Füri et al. 2017), significant amounts of cosmogenic isotopes are present in basalt 15016 minerals. The absence of a primordial component in basalt 15016 vesicles, as well as the gentle crushing performed in this study to avoid damage to the crystal lattice leading to the release of gases from the matrix/minerals, have allowed us to investigate the occurrence of cosmogenic noble gases in basalt 15016 vesicles. By comparing the cosmogenic nuclide contents (He, Ne, Ar, Kr, and Xe) of the vesicles and minerals (derived from crushing experiments of cm-sized samples and laser heating experiments on postcrushing mineral aggregates, respectively), this study brings constraints on the mechanisms of cosmogenic nuclide mobility and loss from minerals and discusses their implications for cosmogenic exposure dating.

SAMPLES AND METHODS

basalt 15016 is a medium-grained basalt composed of subhedral phenocrysts of zoned pyroxene (1–2 mm) and olivine (~1 mm) set in a matrix of subophitic intergrowths of pyroxene and plagioclase (Meyer 2009). In the present study, the term "matrix" refers to the mineral assemblage consisting of both the macrocrysts and the basaltic matrix. Spherical vesicles (up to 5 mm large) make about 50% volume of the basalt. By examining 15 thin sections of basalt 15016 (~300 vesicles), we determined—to a first approximation (Eisenhour 1996)—that the vesicles have a mean diameter of 2.2 ± 0.4 (1SD) mm.

Three cm-sized chips (LP, LR, and LS) of basalt 15016 (m_{LP} = 818.9 mg, m_{LR} = 673.4 mg, and m_{LS} = 414.1 mg) were prepared for vacuum crushing experiments (Fig. 1a). Samples LP and LR (two crushing steps each) were dedicated to Ar, Kr, and Xe isotopic analyses using a Thermofisher© Helix MC Plus mass spectrometer. Sample LS (10 crushing steps in total) was used for He, Ne, Ar, and N_2 isotopes analysis with a Micromass© VG5400 mass spectrometer. Single aliquots of crush residues (a few millimeters in size) of sample LP were handpicked for noble gas and N_2 "bulk" isotopic analysis by static mass spectrometry following CO_2 laser heating extraction (Humbert et al. 2000) (Fig. 1a).

Crushing of Lunar basalt 15016 Chips

Samples were cleaned in an ultrasonic bath filled with acetone, then weighed and loaded into on-line crushers (Zimmermann and Marty 2014). The latter consist of modified high-vacuum angle valves (CF16 flanges), in which a rotation system permits manual adjustment of a bellow extension length, which in turns drives a piston up and down on the sample for crushing

(Fig. 1b). This system allows the crushing intensity to be precisely controlled, notably in the case of soft crushing, and thus leads to reduced blank contributions because of the absence of the wall grinding typically associated with magnetically driven crushers (Zimmermann and Marty 2014). Blanks were monitored by activating the piston in static mode without crushing the sample. Daily standards were run for mass discrimination corrections and determination of the sensitivity and reproducibility of the mass spectrometer.

For samples LP and LR, extracted gases were purified first on two Ti-getters, held at 650 °C for 5 min and then operated at room temperature for the next 5 min. Xe and Kr were separated from the rest of the purification system by trapping them over 10 min on the surface of a Pyrex finger cooled at liquid nitrogen temperature. Ar isotopic measurements were then carried out on the remaining fraction, using an electron multiplier for $^{36–38}$Ar and a Faraday cage for ^{40}Ar. After Ar analysis, the residual Ar in the cold finger was removed by expanding it into the entire extraction line 10 times while keeping the cold finger at liquid nitrogen temperature. During pumping of the line, the glass finger held at liquid nitrogen temperature was isolated from the line to avoid any isotopic fractionation. The glass trap containing Kr and Xe was then heated up and the released gases were exposed once again to two additional hot Ti-getters for final purification. Krypton and xenon isotopes were measured with a Helix MC Plus mass spectrometer by peak jumping on the central dynode electron multiplier AX (CDD).

For each first crushing step, a light mechanical force was applied to the sample by slowly pressing the piston down onto the sample and squeezing it until the first cracks could be heard, thus allowing zones of fragility within the samples to be broken. In this step, most of the gas released was extracted from the vesicles, with little contribution from the matrix. Second crushing steps (samples LP and LR) were carried out by repeatedly crushing the samples until no more cracking was audible. For sample LS, the first crushing steps were likewise gentle but subsequent steps were carried out by applying constant and maximal mechanical squeezing. During these stronger crushing steps, more and more new mineral surfaces were created, thereby increasing the matrix contribution to the gas released, until a coarse powder was obtained.

After crushing, the three powdered samples were recovered for observation. While LS and LR had both been reduced into a fine dust, several mineral aggregates of a few millimeters in size remained in sample 15016 LP (indicative of incomplete crushing). Four subsamples were prepared from these postcrushing aggregates of 15016 LP for bulk measurements by CO_2 laser extraction. Helium, neon, argon, and nitrogen isotopes were measured in two postcrushing aggregates weighing 2.629 and 5.909 mg, while krypton and xenon isotopes were measured in fragments weighing 2.673 and 4.513 mg.

CO_2 Laser Heating of Lunar basalt 15016 Crush Residues

After cleaning in acetone and weighing, the two LP crush residues selected for He, Ne, Ar, and N_2 isotope analysis were loaded into a laser cell connected to the purification line of the Micromass© VG5400 mass spectrometer. The laser chamber was pumped down to 10^{-9} mbar and then heated at 120 °C for several days. Gases were extracted from the samples by heating them with a power-modulated CO_2 infrared (λ = 10.6 μm) laser (Humbert et al. 2000). Daily blanks and standards were run before and during analyses for subsequent blank and mass discrimination corrections. After the high-temperature extraction, the formation of a spherule of molten silicate indicated that the melting temperature of the sample had been reached, and that ≥99% of the gas had been extracted (Humbert et al. 2000). Extracted gases were then split into two calibrated volumes for separate purification and measurement of nitrogen and He-Ne-Ar isotopes, respectively (Hashizume and Marty 2004; Zimmermann et al. 2009; Füri et al. 2015). After purification on Ti sponge getters and two SAES™ Ti-Al getters, Ar was separated from He and Ne using a charcoal finger held at 77 K. Helium (^{3}He measured on an electron multiplier and ^{4}He measured on a Faraday cage) and Ne (all three isotopes measured on an electron multiplier) were sequentially analyzed. Contributions of $^{40}Ar^{++}$ and CO_2^{++} to the ^{20}Ne and ^{22}Ne peaks, respectively, were minimized by exposing the Ne-He gas fraction to another charcoal finger at 77 K and an SAES™ AP-10 getter in contact with the mass spectrometer volume during measurement. The Ne isotope peaks were corrected for these contributions. In parallel, gases were also extracted from the two other LP crush residues selected for Kr and Xe isotope analysis by following the same procedure of extraction. The purification method used was the same as that described in the Crushing of Lunar basalt 15016 Chips section, except that Ar was not analyzed.

RESULTS

Cosmogenic Isotope Abundances in the Matrix and Vesicles

Data for the abundances and isotopic compositions of He, N_2, Ne, Ar, Kr, and Xe in lunar basalt 15016 are given in Tables S1–S8, respectively, in the supporting information. Both the vesicle and matrix gases show intermediate compositions between the pure cosmogenic

endmember and the atmospheric (possibly solar or chondritic) component, but no clear evidence for a primordial component signature could be detected. Table 1 summarizes the abundances of cosmogenic ^{3}He, ^{21}Ne, ^{38}Ar, ^{83}Kr, and ^{126}Xe extracted by crushing (proxy of the vesicle content) and heating (proxy of the matrix content) the samples. By considering ^{3}He, ^{21}Ne, ^{38}Ar, ^{83}Kr, and ^{126}Xe of cosmogenic origin only, we estimate the fractions of these isotopes located in the vesicles relative to bulk contents. Though calibration of the Kr sensitivity of our line is still ongoing and the ^{83}Kr concentrations are only indicative, the vesicle/matrix ratio for cosmogenic Kr can still be estimated.

We find that vesicle gases contain ~0.2% and ~0.02% of the total amount of cosmogenic ^{21}Ne and ^{38}Ar produced over the 300 Ma of cosmic ray exposure, respectively (Table 1). This is in agreement with the higher ^{21}Ne/^{38}Ar ratios found in the vesicles (^{21}Ne/^{38}Ar ~ 8.8) compared to in the matrix (^{21}Ne/^{38}Ar ~ 1.6). This difference is also consistent with lower ^{21}Ne nominal exposure ages than ^{38}Ar ones, as often observed in lunar samples (Signer et al. 1977) and interpreted as evidence for a preferential loss of lighter cosmogenic noble gases over the duration of a sample's exposure, although the exposure ages calculated here for basalt 15016 from ^{21}Ne and ^{38}Ar isotopes are similar within error (Table 1).

Exposure ages derived from ^{3}He, ^{21}Ne, ^{38}Ar, and ^{126}Xe isotopes concentrations in the matrix yield essentially the same result (~350 Ma), notwithstanding that ^{3}He ages appear to be marginally younger than ^{21}Ne and ^{38}Ar ones (Table 1), in agreement with lower nominal exposure ages that are systematically obtained for lunar basalts when using ^{3}He cosmogenic dating (Füri et al. 2017). The proportion of cosmogenic isotopes detected in the vesicles relative to the total abundance of cosmogenic isotopes (i.e., vesicles + matrix) decreases from ^{21}Ne (~0.2%) to ^{83}Kr (~0.002%, see the %vesicles given in Table 1), thus demonstrating a decrease in cosmogenic isotope loss from the light to the heavy isotopes (Signer et al. 1977). However, the fraction of cosmogenic ^{126}Xe detected in vesicles is of the same order of magnitude as that of cosmogenic ^{38}Ar (i.e., ~0.02%) with slightly larger ^{126}Xe/^{38}Ar ratios in the vesicles than in the matrix (Table 1).

Helium and Nitrogen Isotopic Analyses of Lunar basalt 15016

Almost no He was extracted during the crushing experiments, so no ^{3}He was detected. During the laser heating experiments, small but detectable amounts of He were extracted, with helium isotope ratios ranging from $(4.33 \pm 0.84) \times 10^{-4}$ to $(1.90 \pm 0.37) \times 10^{-3}$ (2σ), indicating a cosmogenic contribution (see Table S1). No N was detected from crushing sample LS, but large excesses of cosmogenic ^{15}N were measured during laser extractions (Table S2), with δ^{15}N values reaching 11,300 ± 1400 ‰ (2σ) during melting of the 2.629 mg crush residue.

Neon and Argon Isotopic Analyses of Lunar basalt 15016

For the 10 crushing steps of sample LS, the Ne isotopes tend to fall roughly between the non-cosmogenic (Air/Q/Solar Wind) and the cosmogenic endmembers (green circles in Fig. 2; Table S3). The yellow star in Fig. 2a, which indicates the error-weighted mean isotopic composition of the whole crushing series, does not fall on the mixing line between the atmosphere and the theoretical galactic cosmic rays endmember (GCR, calculated using the 2π exposure model from Leya et al. [2001] for low shielding [0–20 g cm^{-2}] and the basalt 15016 chemical composition summarized by Meyer [2009]). The cosmogenic endmember falls within the range of values expected for the solar cosmic rays (SCRs) component, computed using the models of Reedy (1992) and Trappitsch and Leya (2014) for a rigidity R_0 = 100 MV and an incident particle flux J of 100 protons cm^{-2}. Contrary to Ne, the error-weighted mean isotopic composition of the whole Ar crushing series (yellow star, Fig. 2b) falls exactly on the mixing line between the atmospheric and the GCR components. The SCR component for Ar isotopes, derived from the model of Trappitsch and Leya (2014) using the same assumptions as Ne, is shown in Fig. 2b. Because of the high variability in calculated Ar production rates (mostly dependent on the sample's depth relative to its surface), no clear contribution from SCR-derived Ar isotopes can be derived.

For both Ne and Ar, about 50% of the total amount of gases extracted over the 10 crushing steps of sample LS were released during the first crushing step (Fig. 2c). Likewise, Ar isotopes measured from crushing of samples LP and LR (diamond and hexagon symbols in Fig. 2b, respectively) show that 75% (LP) and 93% (LR) of the ^{36}Ar was released during the first, gentle, step (Fig. 3d), with high ^{38}Ar/^{36}Ar ratios and low ^{40}Ar/^{36}Ar ratios relative to atmosphere (Fig. 2b). The second crushing steps for samples LP and LR yielded low concentrations of gas with elevated ^{38}Ar/^{36}Ar and ^{40}Ar/^{36}Ar ratios, likely pointing to contributions from a cosmogenic and radiogenic component, respectively. Ne and Ar released during high temperature CO_2 laser heating steps are dominated by the GCR component (Figs. 2a and 2b). For Ar, the CO_2 laser heating points plot beyond the expected area for atmospheric, SW/Q, and cosmogenic contributions, likely indicating that a radiogenic component is also contributing (Fig. 2b). For the first fragment (2.63 mg, three extraction steps, red squares in

Table 1. Concentrations (mol g^{-1}) of cosmogenic ^{3}He, ^{21}Ne, ^{38}Ar, ^{83}Kr, and ^{126}Xe extracted during crushing experiments (proxy of the vesicle content) and CO_2 laser extraction series (proxy of the matrix content). $^{21}Ne/^{38}Ar$ and $^{126}Xe/^{38}Ar$ ratios are given when possible. % cosmo = contribution of the pure cosmogenic endmember in percentage. %vesicles = proportion of the cosmogenic isotope in vesicles, calculated as (concentration of the cosmogenic isotope in vesicles)/(concentration of the cosmogenic isotope in vesicles + in the matrix). Calculated exposure ages are based on sample chemical composition (Meyer 2009) and production rates given by Reedy (1981) for ^{3}He, Leya et al. (2001) for ^{21}Ne, and Hohenberg et al. (1978) for ^{38}Ar and ^{126}Xe. Note that our standard calibration for the ^{83}Kr quantities is a work-in-progress, so ^{83}Kr data are only given for an estimation of the fraction of cosmogenic ^{83}Kr in vesicles. [1] = exposure ages reported by Füri et al. (2017) Bold text refers to mean values.

	Mass (g)	^{3}He (mol g^{-1})	^{21}Ne (mol g^{-1})	^{38}Ar (mol g^{-1})	^{83}Kr (mol g^{-1})	^{126}Xe (mol g^{-1})	$^{21}Ne/^{38}Ar$	$^{126}Xe/^{38}Ar$
Vesicles	Crushing				Indicative			
	%cosmo		74%	a: 50%b: 30%	3%	14%		
	0.4141 (LS)	–	4.03×10^{-14}	[a]4.56×10^{-15}	–	–	8.84	–
	0.8189 (LP)	–	–	[b]6.87×10^{-16}	2.25×10^{-19}	1.38×10^{-19}	–	2.01×10^{-04}
	0.6734 (LR)	–	–	[b]1.50×10^{-15}	2.86×10^{-19}	2.27×10^{-19}	–	1.51×10^{-04}
	Mean	–	$\mathbf{4.03 \times 10^{-14}}$	$\mathbf{2.25 \times 10^{-15}}$	$\mathbf{2.55 \times 10^{-19}}$	$\mathbf{1.82 \times 10^{-19}}$	–	$\mathbf{8.11 \times 10^{-05}}$
Matrix	Heating–Melting				Indicative			
	%cosmo		99%	99%	20%	15%		
	0.00263 (LP)	1.68×10^{-10}	1.95×10^{-11}	1.19×10^{-11}	–	–	1.64	–
	0.00591 (LP)	1.63×10^{-10}	2.17×10^{-11}	1.47×10^{-11}	–	–	1.47	–
	0.00267 (LP)				1.57×10^{-14}	6.57×10^{-16}		
	0.00451 (LP)				1.29×10^{-14}	9.63×10^{-16}		
	Mean	$\mathbf{1.70 \times 10^{-10}}$	$\mathbf{2.06 \times 10^{-11}}$	$\mathbf{1.33 \times 10^{-11}}$	$\mathbf{1.43 \times 10^{-14}}$	$\mathbf{8.10 \times 10^{-16}}$	**1.55**	$\mathbf{6.25 \times 10^{-05}}$
	Matrix/Vesicles	–	512	5915	56054	4442	–	–
	%vesicles	–	0.195%	0.017%	0.002%	0.023%		
	Calculated exposure age	336 Ma[1]	378 Ma[1]	361 Ma	~900 Ma	255 Ma		
		325 Ma[1]	422 Ma[1]	445 Ma		373 Ma		

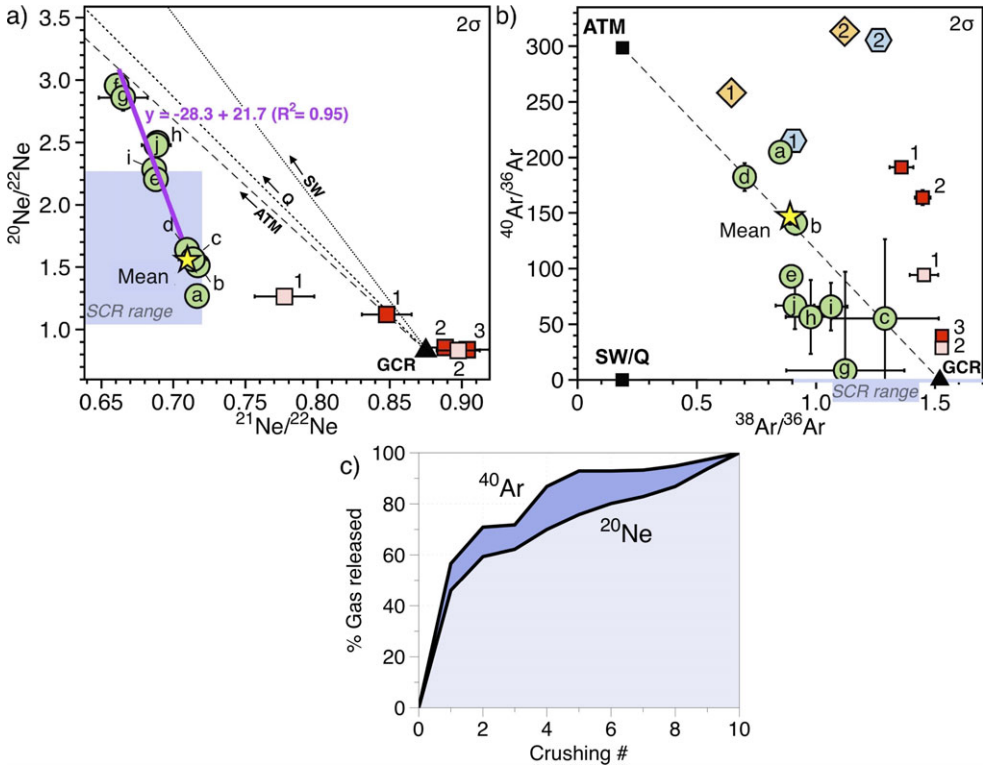

Fig. 2. Light noble gas abundances and isotopic ratios measured in basalt 15016. Yellow stars refer to error-weighted mean isotopic compositions of the crushing series. Letters in circles indicate the crushing steps reported in Tables S3 and S4. Numbers correspond to the heating steps given in Table S3 and S5. a) Neon isotopic composition of lunar basalt 15016 gases extracted by crushing (sample LS, green circle) and by CO_2 laser heating (red [2.629 mg] and light pink [5.909 mg] squares). Pure solar cosmic ray (SCR) range of values (blue area) based on basalt 15016 chemistry (Meyer 2009) and Trappitsch and Leya (2014) model: $^{20}Ne/^{22}Ne$ = (1.04–2.27), $^{21}Ne/^{22}Ne$ = (0.61–0.72). ATM: Terrestrial atmosphere (Ozima and Podosek 2002), $^{20}Ne/^{22}Ne$ = 9.8, $^{21}Ne/^{22}Ne$ = 0.029. GCR: Calculated pure galactic cosmic ray endmember (Leya et al. 2001) based on sample chemistry (Meyer 2009), $^{20}Ne/^{22}Ne$ = 0.83, $^{21}Ne/^{22}Ne$ = 0.875. Error bars are 2σ. b) Argon isotopic composition of lunar basalt 15016 gases extracted by crushing (green circles for sample LS, diamonds and hexagons for sample LP and LR, respectively) and by CO_2 laser heating (red [2.629 mg] and light pink [5.909 mg] squares). Pure solar cosmic ray (SCR) range of values (blue area) based on basalt 15016 chemistry (Meyer 2009) and Trappitsch and Leya (2014) model: $^{40}Ar/^{36}Ar$ = 0, $^{38}Ar/^{36}Ar$ = (0.91–2.24). ATM = terrestrial atmosphere (Lee et al. 2006), $^{40}Ar/^{36}Ar$ = 298.56, $^{38}Ar/^{36}Ar$ = 0.1885. GCR = pure galactic cosmic ray endmember (Hohenberg et al. 1978), $^{40}Ar/^{36}Ar$ = 0, $^{38}Ar/^{36}Ar$ = 1.52. Error bars are 2σ. c) Fraction of ^{22}Ne and ^{36}Ar gradually released over the crushing steps (in percentage). Values are given in Tables S3–S5. (Color figure can be viewed at wileyonlinelibrary.com.)

Figs. 2a and 2b), 81% of the total ^{22}Ne and 79% of the total ^{36}Ar released under CO_2 laser heating were extracted during the melting step. For the second fragment (5.91 mg, two extraction steps, light pink squares in Figs. 2a and 2b), 98% of the total ^{22}Ne and 96% of the total ^{36}Ar were extracted during the melting step.

Ne and Ar from the vesicles were successfully extracted during gentle crushing steps; however, no indigenous magmatic component could be clearly identified as all isotope compositions point to a cosmogenic origin. The latter might be related to cosmogenic loss effects, as has been demonstrated to occur in lunar samples for ^{21}Ne and (to a lesser extent) ^{38}Ar (Frick et al. 1975a, 1975b; Eberhardt et al. 1976; Signer et al. 1977). In this case, the cosmogenic isotopes escaping the minerals might have been stored in the vesicles before being released by crushing. Cosmogenic losses, which have not previously been demonstrated to occur in a measurable way for the heavy noble gases, should thus be negligible for Kr and Xe isotopes, making the potential detection of indigenous magmatic gases more likely.

Krypton and Xenon Isotopic Analyses of Lunar basalt 15016

The Kr isotope ratios measured during crushing experiments of samples LP and LR are distinct from those of the terrestrial atmosphere, in agreement with two-component mixing between the atmosphere and the GCR endmember (Fig. 3a). As observed in the Ne and Ar data, the Kr laser extraction yielded a composition that is closer to the cosmogenic component, with the ^{83}Kr-based proportions of the cosmogenic endmember

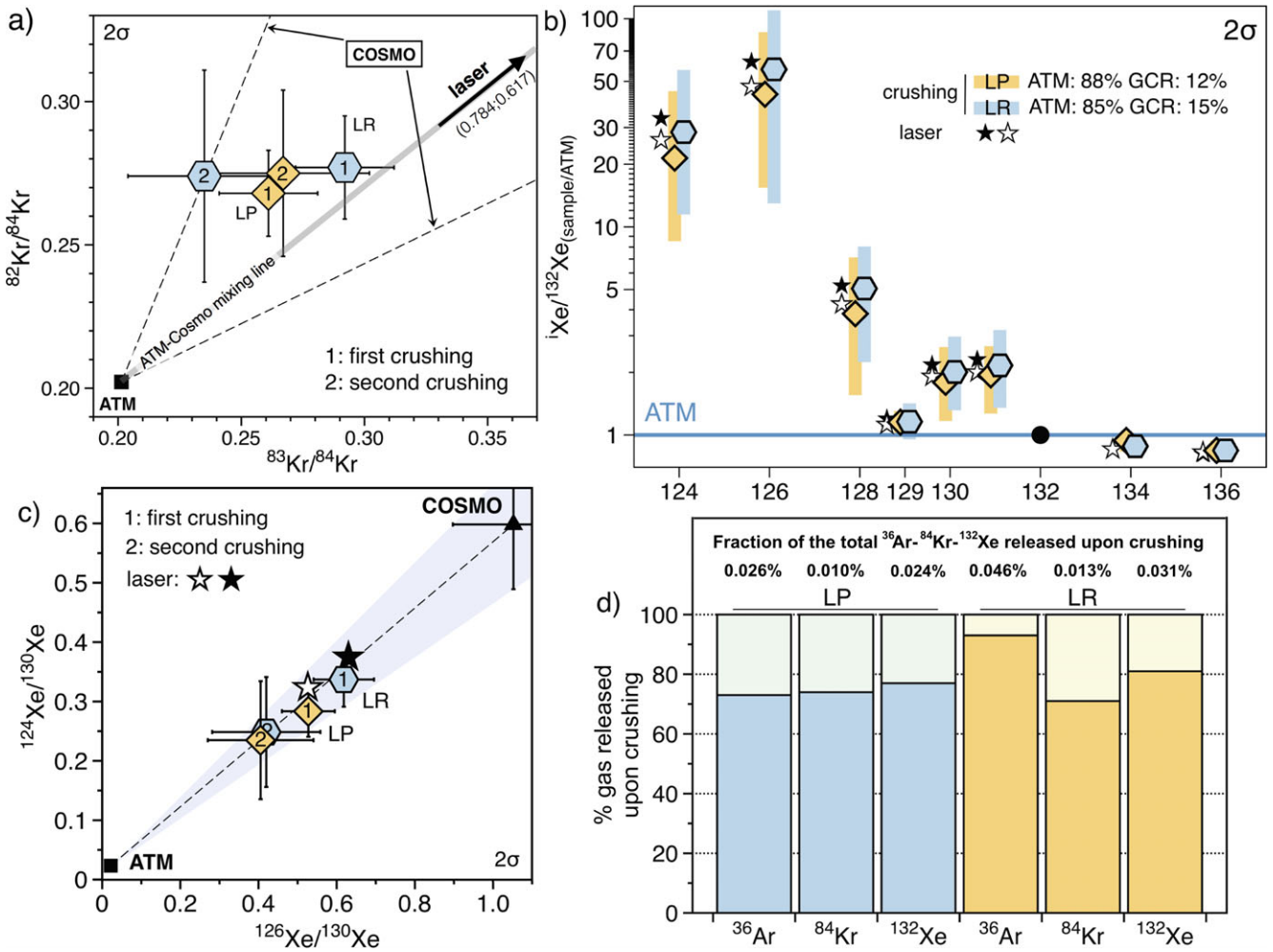

Fig. 3. Heavy noble gas abundances and isotopic ratios measured in basalt 15016. a) Three-isotope diagram of Kr for crushing experiments on LP (diamonds) and LR (hexagons) samples, and for laser extractions (arrow). The laser data plot exactly on the ATM-Cosmo mixing line, with a contribution of the pure cosmogenic endmember estimated at 20% (Table 1). ATM = terrestrial atmosphere (Ozima and Podosek 2002), $^{82}Kr/^{84}Kr$: 0.20217, $^{83}Kr/^{84}Kr$: 0.20136. COSMO = average lunar bulk soils cosmogenic component (Pepin et al. 1995), $^{82}Kr/^{84}Kr$: 2.25 ± 1.44, $^{83}Kr/^{84}Kr$: 3.13 ± 1.96. Error bars are 2σ. b) Isotopic spectra of Xe released during the first crushing step on LP (diamonds) and LR (hexagons) samples, and by laser extraction (black and white stars). Isotopic ratios are normalized to the isotopic composition of atmospheric Xe (Ozima and Podosek 2002) and displayed in log units. Errors bars (2σ) are within the symbols. Vertical bars are the range of theoretical isotopic ratios expected for the given ATM-GCR two endmember mixing models. c) Three-isotope diagram of Xe released during crushing of LP (diamonds) and LR (hexagons) samples and by laser extraction (black and white stars). ATM = terrestrial atmosphere (Ozima and Podosek 2002). COSMO = average lunar bulk soils from Pepin et al. (1995). Error bars are 2σ. d) Fraction of ^{36}Ar, ^{84}Kr, and ^{132}Xe released during the LP and LR crushing experiments (in % relative to the total amount of gas released during the two crushing steps). The first crushing step is shown in the darker color. Values are given in (Tables S4, S6, S7, and S8. (Color figure can be viewed at wileyonlinelibrary.com.)

estimated to be ~3% for the crush extraction and ~20% for the laser heating extraction (Table 1).

For Xe measured during the crushing experiments, the isotopic ratios $^{124–126}Xe/^{132}Xe$ (the two Xe isotopes most sensitive to cosmogenic contribution because of their low initial concentrations and high production rates) are exceptionally high, up to 57 times the atmospheric ratio for the $^{126}Xe/^{132}Xe$ ratio of sample LR (Figs. 3b and 3c). The isotopic spectra measured for samples LP and LR are in excellent agreement with two-component mixing between the terrestrial atmosphere (or SW/Q) and the pure cosmogenic endmember. The mixing proportions are 88% ATM–12% GCR and 85% ATM–15% GCR for LP and LR, respectively (vertical bands, Fig. 3b), assuming mixing between terrestrial atmospheric gases and the cosmogenic endmember for lunar samples with associated errors, given by Pepin et al. (1995). Note that

the $^{134–136}Xe/^{132}Xe$ ratios normalized to terrestrial atmosphere are lower than unity because of a normalization effect, the cosmogenic production rate being higher for the normalizing isotope ^{132}Xe than for $^{134–136}Xe$ (Hohenberg et al. 1978). Xenon released upon laser heating also has a large contribution from the GCR component (Figs. 3b and 3c). Similar to the case of the light noble gases, 74% and 71% of the total ^{84}Kr and 77% and 81% of the total ^{132}Xe released upon crushing of samples LP and LR, respectively, were released during the first (light) crushing step (Fig. 3d). Note that gases detected here in vesicles represent only 0.01% to 0.05% of the total amount of ^{36}Ar, ^{84}Kr, and ^{132}Xe present in the samples, respectively (Fig. 3d). As reported in Table 1, the proportion of cosmogenic ^{36}Ar, ^{83}Kr, and ^{126}Xe detected in the vesicles relative to the total abundance of cosmogenic isotopes (i.e., vesicles + matrix) is ~0.02%, ~0.002%, and ~0.02%, respectively.

While a greater contribution from the GCR component is observed for He, Ne, Ar, and Kr laser extractions relative to the crushing data, the Xe contribution from the atmospheric endmember is still very high during laser heating. This may be related to the fact that new active surfaces were created during the initial crushing of sample LP, so that enhanced abnormal adsorption occurred when the sample was subsequently exposed to atmosphere (Garrison et al. 1987; Hohenberg et al. 2002) before the laser heating experiment. The high precision of our Xe data from laser extractions allowed us to calculate the pure cosmogenic component in our sample by assuming an addition of terrestrial atmosphere or SW-Xe. By comparing the calculated cosmogenic endmember with the average lunar bulk soil cosmogenic component (Pepin et al. 1995), contributions from terrestrial atmosphere and/or SW-Xe might be tentatively distinguished. Our determination of the pure cosmogenic component is in excellent agreement with that of Pepin et al. (1995), but a contribution from either solar or terrestrial Xe cannot be discriminated (Fig. 4).

DISCUSSION

SCR- and GCR-Induced Spallation Reactions

The lunar surface lacks atmospheric and magnetic shields against irradiation by SW and cosmic ray particles. While SW-derived gases are only implanted into the top few tens of nanometers of the rock (e.g., Wieler 1998), cosmic ray-induced spallation reactions triggered by SCRs and GCRs can penetrate lunar soils to depths of a few centimeters and meters, respectively. The rates of Ne isotope production by SCRs at the uppermost rock surface are significantly higher than those by GCRs (e.g., by a factor ~10 for ^{20}Ne; Reedy 1992; Trappitsch and Leya 2014). Consequently, any contribution of SCR-derived neon is expected to result in a noticeable shift in the isotopic signature of the cosmogenic Ne component, as observed here in the LS sample crushing data (Fig. 2a). However, there is no simple explanation as to why SCR and GCR cosmogenic components appear to be separated between two distinct phases in the sample, i.e., vesicles and matrix. Isotopic fractionation during recoil (or diffusion into vesicles) is unlikely the key mechanism since this would favor the light isotopes and would lead to high $^{21}Ne/^{22}Ne$ ratios in the vesicles, which is not observed. An alternative option would be to have preferential production of SCR-derived isotopes at the outermost parts of minerals, where processes affecting mobility toward vesicles could have occurred. However, while this might be a viable hypothesis for a lunar regolith, with individual grains possibly having a higher proportion of SCR than GCR cosmogenic isotopes at the very surface of the grain, this process cannot apply to lunar basalts. Another possibility might be that the sample contains a sizeable amount of sodium, which produces GCR-Ne with a $^{21}Ne/^{22}Ne$ on the order of 0.6. This sodium may be locked into Na-rich minerals that have particularly high cosmogenic Ne mobility or, more likely, may be inherited from the inferred large Na loss that occurred during vesiculation of the sample (Brown et al. 1972; Meyer 2009). The trend toward the mixing line between the noncosmogenic and the pure cosmogenic endmembers would result from a decreasing contribution of SCR-derived isotopes during crushing. The atmospheric contribution that was detected could be related to an underestimation of the blank contribution as crushing proceeded. This could have occurred if microleaks were created in the modified valve (crusher) after strong crushing sequences or if frictions of the rock material on the metal surfaces of the crushing system (notably the plate placed at the bottom of the crusher) caused some atmospheric noble gas to be released (Fig. 1b). However, this effect should also be detected in Ar measurements, which is not the case. An alternative explanation is that some chondritic or solar gases are present in these lunar basalt samples.

Cosmogenic Isotope Loss and Surface Exposure Dating

Cosmogenic isotope analysis and exposure dating involves the measurement of cosmogenic nuclides whose accumulation directly depends on three factors: the depth of production, the time elapsed since the surface exposure event, and the concentrations of target elements for cosmogenic production. Postcrystallization exposure dating assumes that all cosmogenic isotopes produced

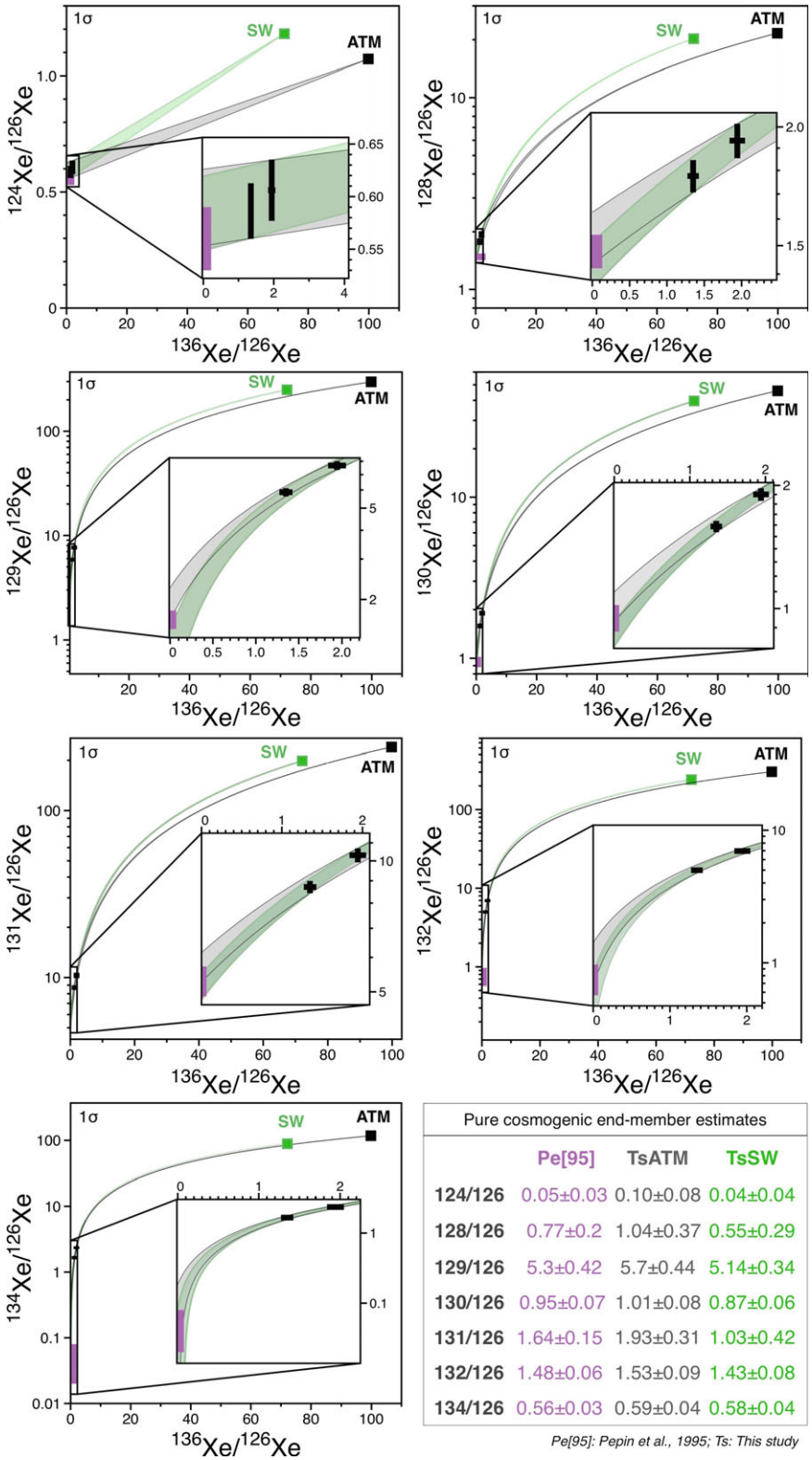

Pure cosmogenic end-member estimates

	Pe[95]	TsATM	TsSW
124/126	0.05±0.03	0.10±0.08	0.04±0.04
128/126	0.77±0.2	1.04±0.37	0.55±0.29
129/126	5.3±0.42	5.7±0.44	5.14±0.34
130/126	0.95±0.07	1.01±0.08	0.87±0.06
131/126	1.64±0.15	1.93±0.31	1.03±0.42
132/126	1.48±0.06	1.53±0.09	1.43±0.08
134/126	0.56±0.03	0.59±0.04	0.58±0.04

Pe[95]: Pepin et al., 1995; Ts: This study

Fig. 4. $^{i}Xe/^{126}Xe$ versus $^{136}Xe/^{126}Xe$ diagrams and determination of the $^{i}Xe/^{126}Xe$ ratios of the pure cosmogenic endmember. The cosmogenic endmember corresponds to the *y*-intercept of the lines drawn through the ATM/SW endmember and the 1σ error envelope of the 15016 data measured by CO_2 laser extraction. The $^{i}Xe/^{126}Xe$ ratios of the pure cosmogenic endmember were derived both from calculations involving ATM (TsATM) or SW (TsATM) and are compared to the average lunar bulk soil cosmogenic component of Pepin et al. (1995). (Color figure can be viewed at wileyonlinelibrary.com.)

over a sample's exposure duration (~300 Ma for basalt 15016; Füri et al. 2017) are preserved and accumulated within the host minerals/rock. One potential problem is the loss of cosmogenic isotopes, which tends to increase with decreasing grain size (at least for mineral grains) and decreasing isotope mass (as evidenced for ^{3}He, ^{21}Ne, and ^{38}Ar) (Signer et al. 1977). Our results confirm that such loss does indeed occur, the predominant release of cosmogenic gases during the first gentle extraction step indicating that their initial location was in the vesicles. If the extracted gases were initially intracrystalline, the amount of gas extracted should have increased with increasing crushing intensity; however, we did not observe it here. The gas measured during the crush experiments must therefore have originally been located in the vesicles, with limited contribution from the matrix.

These results suggest that loss of cosmogenic isotopes occurred for all noble gases, including Xe, during residence time at the lunar surface. The fact that exposure ages derived from ^{3}He, ^{21}Ne, ^{38}Ar, and ^{126}Xe isotope concentrations in the matrix are essentially the same (~350 Ma) indicates that limited cosmogenic loss occurred for all isotopes—a conclusion that is in agreement with the fact that vesicles contain only ~0.2% of the total amount of cosmogenic ^{21}Ne produced over the basalt's exposure. In a first step, as a result of recoil effects, cosmogenic isotopes would have migrated to low-energy retention sites during production. The release of cosmogenic isotopes from the vesicles to outer space through microleaks would then have taken place over time, with kinetic fractionation favoring the escape of the light elements over the heavy ones and, thus, the preferential retention of xenon relative to other noble gases. Higher concentrations of target elements in the walls of vesicles hosted by accessory minerals (opaque minerals—ilmenite and ulvöspinel—as described by Meyer 2009) could have enhanced the trapping of cosmogenic isotopes in the vesicles. Also, note that spallation produces crystal damage over long exposure histories, which will enhance the mobility of cosmogenic isotopes within minerals (Trull et al. 1991).

In the following discussion we investigate diffusion, fracture-related extraction mechanisms, and recoil processes as potential sources of cosmogenic signatures within basalt 15016 vesicles. In particular, the detection of Xe cosmogenic isotopes outside their host minerals (here in the vesicles of the lunar basalt 15016) may indeed require specific production and mobility processes.

Cosmogenic Isotope Loss by Diffusion

Diffusion data are usually interpreted by using the Arrhenius equation (Brady and Cherniak 2010), for which the diffusion coefficient is given by: $D = D_0 \times e^{-(Ea/kT)}$ ($m^2\ s^{-1}$), where D_0 is the maximal diffusion coefficient (at infinite temperature; $m^2\ s^{-1}$), E_a is the activation energy for diffusion (J $atom^{-1}$), T is the absolute temperature (K), and k is the Boltzmann constant. The activation energy (i.e., the minimum energy required to initiate diffusion) increases with the noble gas radius (from He to Xe). Higher diffusivities are thus associated with lighter noble gases (Jackson et al. 2016). According to Cherniak and Watson (2012), even if He is mobile at 1100 °C in olivine (of the order of 1 cm yr^{-1}), it will be nearly immobile at terrestrial surface temperatures. Helium diffusion distances would be smaller than 10 nm at 20 °C over the age of the Earth. The duration of illumination by the Sun of a particular location on the surface of the Moon lasts about 14.8 days, followed by 14.8 days of darkness (the lunar synodic period being 29.53 days). While the temperature on the dark side can fall to −170 °C, the temperature at the lunar surface can reach 115 °C when exposed to sunlight (Malla and Brown 2015). This contrast would imply that the sample spent half of its exposure duration (~150 Myr) heated under vacuum at ~120 °C. According to Cherniak and Watson (2012), the He diffusion distance in olivine is expected to be ~1 μm at 100 °C and over 150 Myr. Even if the diffusion of cosmogenic He in silicate glasses and minerals is several orders of magnitude higher than for inherited He (Trull 1989), a 5 mm radius olivine would lose <0.1% of its cosmogenic He in 10^{14} yr at 20 °C. Temperatures of 50 °C would require nearly 10^{12} yr for an equivalent loss of cosmogenic He (Cherniak and Watson 2012). According to Cherniak et al. (2014), 100 μm radius olivine grains would experience less than 1% Ne loss over durations of the order of the age of the Earth at 150 °C. Melcher et al. (1982) determined an upper limit of 3×10^{-16} $cm^2\ s^{-1}$ for the Xe diffusion coefficient in forsterite at 1400 °C, decreasing at around 5×10^{-19} $cm^2\ s^{-1}$ at 900 °C (assuming a plausible activation energy of 50 kcal $mole^{-1}$). Even at ~120 °C, insufficient Xe and lighter noble gases would diffuse through minerals to account for the cosmogenic loss effects detected here.

Yokochi et al. (2005) demonstrated that up to 25% of the matrix-sited helium could be extracted by prolonged crushing of terrestrial olivine. However, their crushing system and procedure (an extensive series of 100 strokes min^{-1}) are not comparable with our method, and only prolonged crushing series were able to remove matrix-sited isotopes in their experiments. Blard et al. (2008) pointed out that temperature-enhanced ($T > 300$ °C) volume diffusion could play a major role in controlling the release of cosmogenic He during crushing. In the present work, the first crushing

steps were manually controlled to be gentle and thus caused no increase in temperature. Nevertheless, most of the gas extracted over the crushing series was released during this step. A smaller amount of gas was released during the subsequent and stronger crushing steps, in which the rate of fracture-related extraction should increase. Fracture-related and/or diffusive extraction mechanisms are therefore unlikely to be the source of the cosmogenic signatures measured during the present crushing experiments.

Cosmogenic Isotope Loss by Recoil Effects

Recoil processes may be the key mechanism by which cosmogenic isotopes are transferred from the matrix into the vesicles. When a high-energy particle induces a nuclear reaction, the nuclide produced has a specific energy due to momentum conservation, termed the recoil energy. To dissipate this energy, the cosmogenic nuclide travels a short distance within the target grain until it stops completely. Through this process, some of the cosmogenic nuclides might be lost from the host grain, before diffusing in intergrain regions and finally into vesicles. Recoil loss effects were studied in detail in the context of cosmogenic dating of small extraterrestrial samples (e.g., micrometeorites and interplanetary dust particles [Trappitsch and Leya 2013], μm-sized presolar silicon carbide grains [Ott et al. 2009]), for which recoil loss can dramatically affect the retention rate of spallation-produced isotopes. While recoil distances for He range from ~20 μm (Heck et al. 2009) up to 100 μm, the recoil distances for ^{21}Ne and ^{126}Xe are much smaller, in the range of ~2.5 μm (Ott and Begemann 2000; Ott et al. 2009; Trappitsch and Leya 2013) and 0.2–0.5 μm (Ott and Begemann 2000; Ott et al. 2005), respectively. Such ranges of values have been compiled from analyses of SiC grain-size fractions of spallation isotopes produced by irradiation with 1.6 GeV protons (Ott et al. 2009), physical models based on nuclear reactions codes (Trappitsch and Leya 2013), and irradiation experiments of Ba glass targets with about 1190 and 268 MeV protons (Ott et al. 2005). Because the recoil range of spallation for Xe is shorter than that of lighter noble gases, Xe has been suggested to be the best tool for dating presolar silicon carbide. In extreme contrast, recoil loss of cosmogenic ^{3}He is significant even for grains of a hundred microns in size (Trappitsch and Leya 2013).

We propose a semiquantitative estimate of what should be expected in vesicles in terms of cosmogenic ^{21}Ne and ^{126}Xe by recoil loss (details of this calculation are given in the supporting information). We considered a volume of basalt 15016 of 1000 cm^3, in which 50% of the volume is made up of vesicles, and the other 50% minerals with a homogeneous chemistry and a mean diameter of 1 mm (as given by Meyer 2009). Recoil distances for ^{21}Ne and ^{132}Xe were taken to be 2.5 and 0.2 μm, respectively. This calculation could not be applied to Kr since, to our knowledge, no data exist in the literature for the recoil distance of Kr. We then determine the volume of minerals in which cosmogenic isotope loss by recoil could occur and obtained values of 7463 mm^3 for ^{21}Ne and 600 mm^3 for ^{126}Xe. However, only a fraction of the cosmogenic isotopes produced within these volumes will actually escape from the minerals. This is due to the fact that the recoil process can occur in any direction within the mineral. Based on geometric considerations (see supporting information for further details), we predict that ~18% of the cosmogenic isotopes produced within the volume of minerals in which cosmogenic isotope loss by recoil occurs will indeed escape from the minerals. Taking these data together, we conclude that 0.272% and 0.022% of the total cosmogenic ^{21}Ne and ^{126}Xe, respectively, would escape from the host minerals by recoil—values which are in excellent agreement with the fraction of cosmogenic ^{21}Ne (0.2%) and ^{126}Xe (0.02%) detected here in the basalt 15016 vesicles. The same calculation can be made for grain sizes ranging from 0.1 mm to 1 mm in radius. We find that, although the fraction of ^{21}Ne lost to the vesicles becomes significant (≥1%) for mean grain radii <0.2 mm, ^{126}Xe loss is still <0.2% for a mean grain radius of 0.1 mm (Fig. S1 in supporting information). Thus, contrary to the light noble gases, heavy noble gas cosmogenic isotope loss by recoil would still be negligible for fine-grained rocks. This simple model we propose does not explain the observed off-the-trend behavior of Xe, which shows enhanced proportion of cosmogenic ^{126}Xe in vesicles relative to the lighter noble gas elements. However, it supports the recoil process as a plausible mechanism for cosmogenic isotope loss from minerals and storage in vesicles, with little loss to space by diffusion.

The estimated rates for cosmogenic isotope loss, as suggested here, suffer from several caveats that are difficult to address accurately due to the large uncertainties regarding the processes controlling the mobility of cosmogenic nuclides within minerals. For instance, it is assumed that an atom recoiled into a vesicle will remain there until it is either lost to space through diffusion, or released by crushing. However, since vesicles are essentially vacuums, energy loss within them is expected to be very limited and atoms recoiled into a vesicle would potentially have enough energy to get reimplanted into the other side of vesicles. This process would preferentially occur for the light elements (He, Ne), entering vesicles with greater energies than the heavy elements, which would be arrested to a greater degree within minerals during recoil. Limited

reimplantation of Xe cosmogenic nuclides entering intergrain joints and/or vesicles may account for the enhanced proportion of cosmogenic ^{126}Xe in the vesicles relative to lighter noble gases. Physical models of cosmogenic production with recoil effects based on nuclear reaction codes (Trappitsch and Leya 2013), as well as experimental investigations of cosmogenic nuclide production by irradiation experiments of glass targets with protons (Ott et al. 2005) appear to be promising avenues of investigation to further constrain the mechanisms occurring during cosmogenic nuclide production and mobility.

CONCLUSIONS

Noble gas and nitrogen isotopes in lunar basalt 15016 were released from vesicles by under-vacuum crushing and from the matrix by heating millimeter-sized crush residues with a CO_2 laser. Both sets of data are consistent with a mixture of atmospheric (or SW/Q) and cosmogenic (including SCR-derived isotopes) components. No indigenous magmatic lunar component could be clearly identified. The detection of cosmogenic isotopes in the vesicles of basalt 15016 indicates the occurrence of specific production and/or mobility processes. Cosmogenic isotope loss from minerals by recoil effects, and subsequent diffusion from vesicles to outer space, is a potential source for cosmogenic isotope loss to space over the duration of exposure. By assuming that no loss to space occurred, i.e., that all of the cosmogenic isotopes that escaped from the minerals were retained in the vesicles of basalt 15016, we conclude that ~0.2%, ~0.02%, ~0.002%, and ~0.02% of the amount of cosmogenic ^{21}Ne, ^{38}Ar, ^{83}Kr, and ^{126}Xe, respectively, escaped from minerals. This indicates that cosmogenic losses over exposure durations on the order of hundreds of millions of years would not significantly affect the calculated exposure ages for basaltic rocks. Interestingly, cosmogenic loss, known to be significant for ^{3}He and ^{21}Ne and to a lesser extent for ^{36}Ar (Signer et al. 1977), also occurs for the heaviest noble gases, including Xe. Based on a simple model of basalt 15016 cosmogenic loss by recoil, we conclude that this process alone could account for the presence of the cosmogenic isotopes that we detected in vesicles. Although light noble gas cosmogenic isotope loss by recoil would be significant in fine-grained rocks, cosmogenic loss by recoil would remain negligible for the heavy noble gases. In this study, the enhanced proportion of cosmogenic ^{126}Xe in vesicles relative to lighter elements may be related to kinetic fractionation processes. In this case, higher rates of escape from the vesicles to space for the lighter elements would account for the preferential retention of Xe isotopes within the intergrain joints and vesicles.

Acknowledgments—We are grateful to NASA and CAPTEM for allocation of these precious Apollo samples. Evelyn Füri, Michael Broadley, and Laurent Zimmermann are thanked for fruitful discussions. Reto Trappitsch kindly provided Excel files that allowed us to make calculations of the Ne and Ar SCR components. We thank R. Wieler, P. Heck, and an anonymous reviewer for their constructive comments as well as M. Caffee for his careful editorial handling. This study was supported by the European Research Council (grants no. 267255 and 695618). This is CRPG contribution #2528.

Editorial Handling—Dr. Marc Caffee

REFERENCES

Barker C. 1974. Composition of the gases associated with the magmas that produced rocks 15016 and 15065. Proceedings, 5th Lunar Science Conference. pp. 1737–1746.

Bekaert D. V., Avice G., Marty B., Henderson B., and Gudipati M. S. 2017. Stepwise heating of lunar anorthosites 60025, 60215, 65315 possibly reveals an indigenous noble gas component on the Moon. *Geochimica et Cosmochimica Acta* 218:114–131.

Blard P. H., Puchol N., and Farley K. A. 2008. Constraints on the loss of matrix-sited helium during vacuum crushing of mafic phenocrysts. *Geochimica et Cosmochimica Acta* 72:3788–3803.

Brady J. B. and Cherniak D. J. 2010. Diffusion in minerals: An overview of published experimental diffusion data. *Reviews in Mineralogy and Geochemistry* 72:899–920.

Brown G. M., Emeleus C. H., Holland G. J., Peckett A., and Phillips R. 1972. Mineral-chemical variations in Apollo 14 and Apollo 15 basalts and granitic fractions. Proceedings, 3rd Lunar Science Conference. pp. 141–157.

Cherniak D. J. and Watson E. B. 2012. Diffusion of helium in olivine at 1 atm and 2.7 GPa. *Geochimica et Cosmochimica Acta* 84:269–279.

Cherniak D. J., Thomas J. B., and Watson E. B. 2014. Neon diffusion in olivine and quartz. *Chemical Geology* 371:68–82.

Colson R. O. 1993. Graphite solubility and co-vesiculation in basalt-like melts at one-ATM. Proceedings, 24th Lunar and Planetary Science Conference. pp. 321–322.

Eberhardt P., Eugster O., Geiss J., Groegler N., Guggisberg S., and Moergeli M. 1976. Noble gases in the Apollo 16 special soils from the East-West split and the permanently shadowed area. Proceedings, 7th Lunar Science Conference. pp. 563–585.

Eisenhour D. D. 1996. Determining chondrule size distributions from thin-section measurements. *Meteoritics & Planetary Science* 31:243–248.

Eugster O. 2003. Cosmic-ray exposure ages of meteorites and lunar rocks and their significance. *Chemie der Erde-Geochemistry* 63:3–30.

Frick U., Baur H., Funk H., and Signer P. 1975a. Diffusive loss of volume correlated He and NE from 15421 soil feldspar (abstract). 6th Lunar and Planetary Science Conference. p. 273.

Frick U., Baur H., Ducati H., Funk H., Phinney D., and Signer P. 1975b. On the origin of helium, neon, and argon isotopes in sieved mineral separates from an Apollo 15 soil. Proceedings, 6th Lunar Science Conference. pp. 2097–2129.

Füri E., Barry P. H., Taylor L. A., and Marty B. 2015. Indigenous nitrogen in the Moon: Constraints from coupled nitrogen–noble gas analyses of mare basalts. *Earth and Planetary Science Letters* 431:195–205.

Füri E., Deloule E., and Trappitsch R. 2017. The production rate of cosmogenic deuterium at the Moon's surface. *Earth and Planetary Science Letters* 474:76–82.

Garrison D. H., Olinger C. T., Hohenberg C. M., and Goswami J. N. 1987. Surface-correlated noble gases from grain-size separates of Kapoeta. *Meteoritics* 22:382.

Garvin J. B., Head J. W., and Wilson L. 1982. Magma vesiculation in Apollo 15 Mare basalts: Observations and theory. Proceedings, 13th Lunar and Planetary Science Conference. pp. 255–256.

Goldberg R. H., Tombrello T. A., and Burnett D. S. 1976. Fluorine as a constituent in lunar magmatic gases. Proceedings, 7th Lunar and Planetary Science Conference. pp.1597–1613).

Hashizume K. and Marty B. 2004. Nitrogen isotopic analyses at the sub-picomole level using an ultra-low blank laser extraction technique. *Handbook of Stable Isotope Analytical Techniques* 1:361–375.

Heck P. R., Gyngard F., Ott U., Meier M. M., Ávila J. N., Amari S., Zinner E. K., Lewis R. S., Baur H., and Wieler R. 2009. Interstellar residence times of presolar SiC dust grains from the Murchison carbonaceous meteorite. *The Astrophysical Journal* 698:1155.

Hohenberg C. M., Podosek F. A., Shirck J. R., Marti K., and Reedy R. C. 1978. Comparisons between observed and predicted cosmogenic noble gases in lunar samples. Proceedings, 9th Lunar and Planetary Science Conference. pp. 2311–2344.

Hohenberg C. M., Thonnard N., and Meshik A. 2002. Active capture and anomalous adsorption: New mechanisms for the incorporation of heavy noble gases. *Meteoritics & Planetary Science* 37:257–267.

Humbert F., Libourel G., France-Lanord C., Zimmermann L., and Marty B. 2000. CO_2-laser extraction-static mass spectrometry analysis of ultra-low concentrations of nitrogen in silicates. *Geostandards Newsletter* 24:255–260.

Jackson C. R., Shuster D. L., Parman S. W., and Smye A. J. 2016. Noble gas diffusivity hindered by low energy sites in amphibole. *Geochimica et Cosmochimica Acta* 172:65–75.

Lee J. Y., Marti K., Severinghaus J. P., Kawamura K., Yoo H. S., Lee J. B., and Kim J. S. 2006. A redetermination of the isotopic abundances of atmospheric Ar. *Geochimica et Cosmochimica Acta* 70:4507–4512.

Leya I., Neumann S., Wieler R., and Michel R. 2001. The production of cosmogenic nuclides by galactic cosmic-ray particles for 2π exposure geometries. *Meteoritics & Planetary Science* 36:1547–1561.

Malla R. B. and Brown K. M. 2015. Determination of temperature variation on lunar surface and subsurface for habitat analysis and design. *Acta Astronautica* 107:196–207.

Melcher C. L., Burnett D. S., and Tombrello T. A. 1982. Measurement of xenon diffusion following ion implantation into olivine. Proceedings, 13th Lunar and Planetary Science Conference. pp. 509–510.

Meyer C. 2009. Lunar sample compendium. https://curator.jsc.nasa.gov/lunar/lsc/index.cfm. Accessed March 6, 2018.

Ott U. and Begemann F. 2000. Spallation recoil and age of presolar grains in meteorites. *Meteoritics & Planetary Science* 35:53–63.

Ott U., Altmaier M., Herpers U., Kuhnhenn J., Merchel S., Michel R., and Mohapatra R. K. 2005. Spallation recoil II: Xenon evidence for young SiC grains. *Meteoritics & Planetary Science* 40:1635–1652.

Ott U., Heck P. R., Gyngard F., Wieler R., Wrobel F., Amari S., and Zinner E. 2009. He and Ne ages of large presolar silicon carbide grains: Solving the recoil problem. *Publications of the Astronomical Society of Australia* 26:297–302.

Ozima M. and Podosek F. A. 2002. *Noble gas geochemistry*. Cambridge, UK: Cambridge University Press.

Pepin R. O., Becker R. H., and Rider P. E. 1995. Xenon and krypton isotopes in extraterrestrial regolith soils and in the solar wind. *Geochimica et Cosmochimica Acta* 59:4997–5022.

Reedy R. C. 1981. Cosmic-ray-produced stable nuclides: Various production rates and their implications. Proceedings, 12th Lunar and Planetary Science Conference. pp. 871–873.

Reedy R. C. 1992. Solar-proton production of neon and argon (abstract). 23rd Lunar and Planetary Science Conference. p. 1133.

Sato M. 1979. The driving mechanism of lunar pyroclastic eruptions inferred from the oxygen fugacity behavior of Apollo 17 orange glass. Proceedings, 10th Lunar and Planetary Science Conference. pp. 311–325.

Signer P., Baur H., Derksen U., Etique P., Funk H., Horn P., and Wieler R. 1977. Helium, neon, and argon records of lunar soil evolution. Proceedings, 8th Lunar Science Conference. pp. 3657–3683.

Trappitsch R. and Leya I. 2013. Cosmogenic production rates and recoil loss effects in micrometeorites and interplanetary dust particles. *Meteoritics & Planetary Science* 48:195–210.

Trappitsch R. and Leya I. 2014. Depth-dependent solar cosmic ray induced cosmogenic production rates (abstract #1894). 45th Lunar and Planetary Science Conference. CD-ROM.

Trull T. W. 1989. Diffusion of helium isotopes in silicate glasses and minerals: Implications for petrogenesis and geochronology (No. WHOI-89-15). Woods Hole, Massachusetts: Woods Hole Oceanographic Institution.

Trull T. W., Kurz M. D., and Jenkins W. J. 1991. Diffusion of cosmogenic ^{3}He in olivine and quartz: Implications for surface exposure dating. *Earth and Planetary Science Letters* 103:241–256.

Wieler R. 1998. The solar noble gas record in lunar samples and meteorites. *Space Science Reviews* 85:303–314.

Wieler R. 2016. Do lunar and meteoritic archives record temporal variations in the composition of solar wind noble gases and nitrogen? A reassessment in the light of Genesis data. *Chemie der Erde-Geochemistry* 76:463–480.

Yokochi R., Marty B., Pik R., and Burnard P. 2005. High ^{3}He/^{4}He ratios in peridotite xenoliths from SW Japan revisited: Evidence for cosmogenic ^{3}He released by vacuum crushing. *Geochemistry, Geophysics, Geosystems* 6.

Zimmermann L. and Marty B. 2014. Méthodes d'extraction des gaz rares sous ultravide. Techniques de l'ingénieur, j6632.

Zimmermann L., Burnard P., Marty B., and Gaboriaud F. 2009. Laser ablation (193 nm), purification and determination of very low concentrations of solar wind nitrogen implanted in targets from the Genesis spacecraft. *Geostandards and Geoanalytical Research* 33:183–194.

SUPPORTING INFORMATION

Additional supporting information may be found in the online version of this article:

Data S1. Data S1 contains eight tables listing the noble gas and nitrogen abundances and isotopic ratios measured in this study and discussed in the main text. This supporting information also contains an explanation of our semi-quantitative estimate of what should be expected in vesicles for 21Ne and 126Xe by recoil loss (Fig. S1 and Table S9).